Charge transfer dynamics and photoconductive properties of ZnO nanowires functionalized with carbon dots

Davide Cammi[1*], Kseniia Zimmermann[1], René Gorny[1], Angelina Vogt[1], Frank Dissinger[2], Alaa Eldin Gad[1], Nicolai Markiewcz[1], Andreas Waag[1], Joan Daniel Prades[3,4], Carsten Ronning[5], Siegfried R. Waldvogel[2], Tobias Voss[1]

[1] Institute of Semiconductor Technology and Laboratory for Emerging Nanometrology (LENA), TU Braunschweig University of Technology, Hans-Sommer-Straße 66, D-38106 Braunschweig, Germany

[2] Institute of Organic Chemistry, Johannes Gutenberg University Mainz, Duesbergweg 10-14, D-55128 Mainz, Germany

[3] MIND, Department of Electronic & Biomedical Engineering, Universitat de Barcelona, C/ Martí i Franquès 1, E-08028 Barcelona, Spain

[4] Institute of Nanoscience and Nanotechnology (IN^{2}UB), Universitat de Barcelona, C/ Martí i Franquès 1, E-08028 Barcelona, Spain

[5] Institute of Solid State Physics, Friedrich Schiller University Jena, Max-Wien-Platz 1, D-D-07743 Jena, Germany

*corresponding author: d.cammi@tu-braunschweig.de

Abstract

We report on the surface functionalization of ZnO nanowire (NW) arrays by attachment of carbon nanodots (C-dots) stabilized by polyethylenimine. The photoconductive properties of the ZnO NWs / C-dots devices were investigated under photoexcitation with photon energies below and above the ZnO bandgap. The results indicate an increased photoresponse of the functionalized devices in the visible spectral range, as well as enhanced UV photoconductivity. This is attributed to the fast injection of photoexcited electrons from the C-dots into the conduction band of the ZnO NWs, and the subsequent slower desorption of molecular species from the NW surface, which reduces the surface depletion region in the NWs. The surface functionalization

of the ZnO NWs by carbon nanodots also impacts the dynamics of the photocurrent decay, inducing a slower relaxation of the photogenerated charge carriers.

Introduction

The design of hybrid devices based on nanostructured materials is a crucial issue in several fields of modern nanotechnology, since it offers the opportunity to achieve enhanced device performance and novel functionalities [1, 2, 3, 4, 5]. In optoelectronic applications, the successful combination of complementary material properties allows, for instance, obtaining high photon absorption and conversion efficiencies into photogenerated charge carriers, as well as efficient charge collection at the electrodes. In this respect, a significant example is the assembly of nanostructured dye-sensitized solar cells, which were introduced in 1991 by O'Regan and Grätzel [6]. The dye is characterized by a suitable absorbance in the visible spectral range and acts as a photosensitizer, providing photogenerated electrons to the TiO_2 electrode. The latter favors an efficient collection of the charge carriers, being characterized by a wide band gap of 3.2 eV and high electron mobility.

In the past decade, huge interest has been devoted to the development of such hybrid devices, including ZnO nanowires (NWs) functionalized with colloidal semiconductor quantum dots (QDs) [7, 8, 9]. ZnO is a metal oxide semiconductor with a wide band gap of 3.37 eV at room temperature, unintentional n-type conductivity and high electron mobility. Additionally, it is biocompatible and can be synthetized at low costs by a variety of physical and chemical methods [10, 11, 12]. Due to unique geometrical properties such as large surface-to-volume ratio and aspect ratio as well as excellent crystalline quality, ZnO NWs provide a direct electrical pathway for charge carriers and an optimal surface morphology for the attachment of nanostructured sensitizers.

Semiconductor quantum dots (QDs) have shown remarkable advantages as photosensitizers compared to traditional organic dyes, including higher stability, size-tunable energy gap, high absorption coefficients and the potential to generate multiple electron-hole pairs by absorption of a single photon [13, 14, 15]. The surface functionalization of ZnO NWs with semiconductor QDs of various material composition and sizes has allowed for developing nanoscale solar cells and photodetectors with increased absorption in the visible spectral range as well as fast charge transfer dynamics in the range of ps at the interface between the NW and the QD [16, 17]. However, most of commonly exploited colloidal semiconductor QDs contain toxic elements such as cadmium, selenium, and/or nickel, which constitute a serious environmental issue for the large-scale applications of such hybrid devices. Therefore, intense research efforts are currently devoted to the synthesis and investigation of alternative nanostructured material systems.

Among those, carbon nanodots (C-dots) constitute a novel class of nanoparticles characterized by excellent properties such as low toxicity, chemical stability, tunable absorption and luminescence as well as up-conversion fluorescence [18, 19, 20]. In particular, their optical properties can be tailored by doping or surface functionalization with various molecules. For these reasons, the design and development of hybrid solar cells and photodetectors consisting of ZnO NWs functionalized with C-dots are extremely attractive for the future development of sustainable “green” optoelectronics.

In the present work, we synthesized nanostructured hybrid devices consisting of a ZnO NW array grown on interdigitated finger electrodes on top of a sapphire substrate, and C-dots stabilized with polyethylenimine molecules. The C-dots were anchored onto the NW surface by chemical bonding between the outgoing amino groups of the C-dots stabilizer and the zinc ions at the surface of the NW [21]. The photoconductive properties of the functionalized devices were investigated upon selective light excitation with photon energies below and above the band gap of the ZnO. Compared to the pristine ZnO NWs, we demonstrated both increase of

the device's photoresponse in the visible spectral range as well as enhanced UV photoconductivity. This is attributed to the fast injection of photoexcited electrons from the C-dots into the conduction band of the ZnO NWs, and the subsequent slower desorption of molecular species from the NW surface, which reduces the surface depletion region in the NWs. Furthermore, we discuss the impact of the surface functionalization of the ZnO NWs on the dynamics of the charge-carrier relaxation.

Experimental section

ZnO NW arrays were produced according to the following procedure. At first, interdigitated finger electrodes were defined on a sapphire substrate by means of photolithography and thermal deposition of Ti (30 nm) and Au (300 nm). Every electrode finger had a width of 59 µm and was separated from the direct neighbor by a gap of 118 µm (Figure 1 (a)). Subsequently, a photoresist layer was applied on the substrate and processed in order to limit the following growth of the NWs to the area spanned by the interdigitated electrode pattern (2.0 mm x 2.5 mm). A ZnO seed layer for the NW growth was then deposited on the substrate by DC sputtering using a Zn target in high purity argon (99.999 %), and subsequent Zn oxidation by thermal annealing in air at 500 °C for 1 hour. The subsequent growth of the NWs was then performed by means of an established hydrothermal method [22]. Finally, the devices were annealed for 1 hour at 500 °C in air, in order to obtain low-resistive ohmic contacts. Figure 1 (b) shows an optical microscope image of a typical ZnO NW device. A scanning electron microscope (SEM) image of a pristine device (Figure 1 (c)) shows a dense film of nearly vertical NWs with average diameters of 150 – 200 nm over the full 2.0 x 2.5 mm area.

The C-dots were synthesized via pyrolysis according to a reported protocol [23]. At first, 2.0 g citric acid monohydrate (Sigma-Aldrich) and 0.5 g polyethylenimine (ethylenediamine branched, $M_w \sim 800$, Sigma-Aldrich) were dissolved in 15 mL of double-distilled water. The

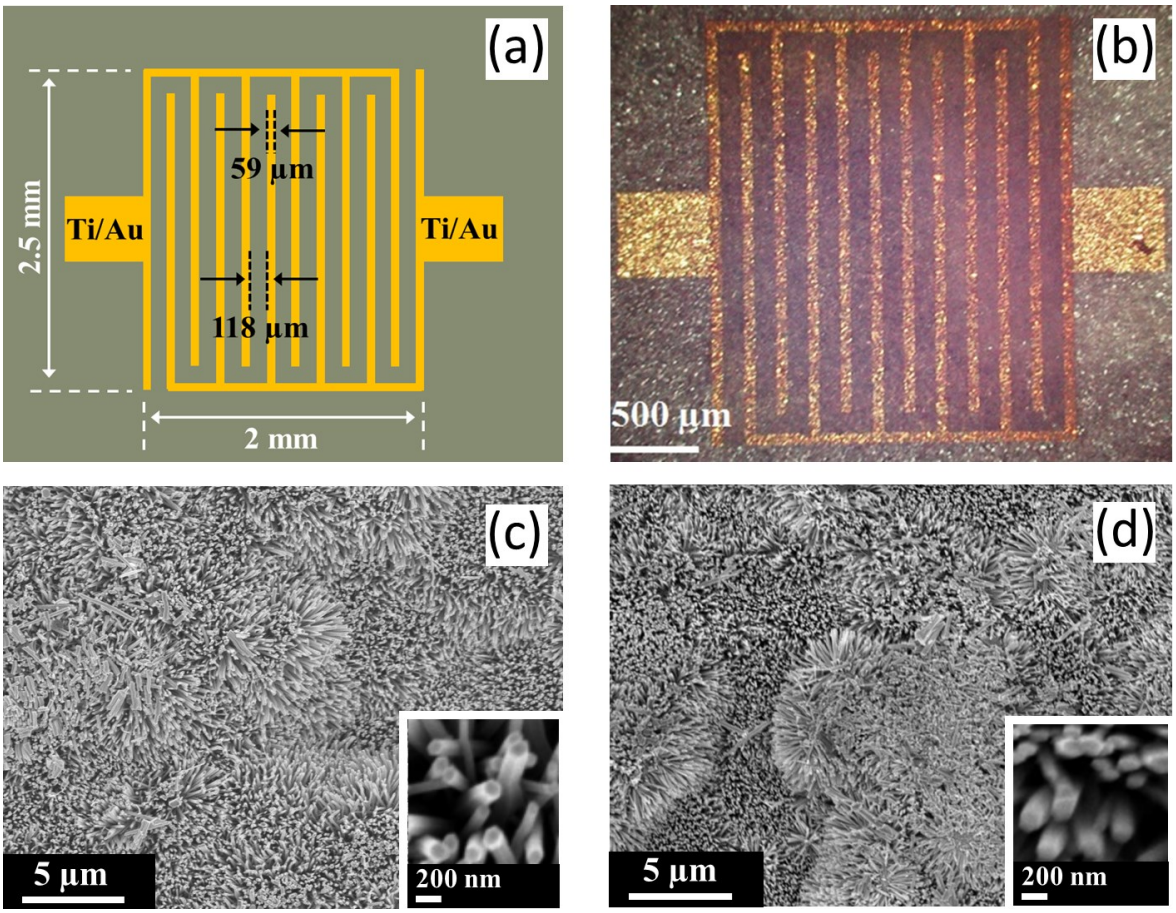

Figure 1. (a) Schematic representation of interdigitated finger electrodes on a sapphire substrate. (b) Optical microscope image of a pristine ZnO nanowire array grown on the finger electrode pattern. (c) Scanning electrode microscope image of a dense film of nearly vertical ZnO nanowires before functionalization. (d) Scanning electrode microscope image of the ZnO nanowires after surface functionalization with carbon nanodots in aqueous solution with pH 4.

resulting solution was then heated to 180 °C in an open beaker. As soon as the solvent was almost completely evaporated and a yellow gel was formed, 2 mL of double-distilled water were added, in order to prevent it from scorching. This procedure was repeated five times until the color changed to orange. This afforded a total heating time of about 20 min. The C-dots were purified by silica column chromatography with 0.01 M aqueous HCl as eluent, neutralized with solid $NaHCO_3$ and freeze-dried. By adding distilled water, HCl, or NaOH, C-dot solutions with a mass concentration of 0.08 % and a pH of 1, 4, or 9 were obtained. Then, 45 µL of the

solution were dropped onto the NW arrays, which were kept in air for several hours until the complete evaporation of the volatiles. In the following, unless the pH value is explicitly mentioned, we will always refer to the solution with pH 4. Figure 1 (d) shows an SEM image of a functionalized device. No significant modification of the NW film morphology can be observed with respect to the pristine device (Figure 1 (c)), indicating the absence of strong etching or corrosion effects.

The optical properties of the C-dots in solution and both the pristine and functionalized devices were investigated by means of UV-Vis absorption and photoluminescence (PL) spectroscopy. The absorption measurements were carried out with a UV-Vis-NIR spectrophotometer (Jasco, model V-670), while the PL measurements were performed by using a continuous wave He-Cd laser as a light excitation source (photon energy 3.81 eV).

The electrical characterization of the devices was conducted in air at room temperature by using a source-measure unit (Keithley, model 2400) and measuring the electric current under application of a voltage difference between the electrodes. A xenon lamp equipped with a 200 mm monochromator was used to generate wavelength-tunable excitation light with bandwidth of around 10 nm at each center wavelength between 600 nm and 390 nm. The excitation intensity was around 40 $\mu W / cm^2$ in the blue and red spectral regions, with a peak value of 80 $\mu W / cm^2$ in the green one.

Results and discussion

The normalized absorption and PL spectra of the as-prepared C-dots in solution are shown in Figure 2. The absorption spectrum, in logarithmic scale, is normalized with respect to the maximum of a broad peak at around 5.6 eV. An additional absorption peak is centered at 3.4 eV and presents a shoulder, which extends into the visible spectral range. The main absorption peak

with maximum at 5.6 eV is assigned to electronic transitions from the highest occupied molecular orbital (HOMO) to the lowest unoccupied molecular orbital (LUMO) in the aromatic domains in the core of the C-dots [24, 25]. Such electronic transitions are schematically indicated in Figure 2 as π - π^*. The broadness of this peak is attributed to the presence of aromatic domains with slightly different size and correspondingly different separation between the HOMO and the LUMO [20]. The absorption peak with maximum at 3.4 eV is instead ascribed to electronic transitions occurring at the surface of the C-dots [24, 25]. These transitions involve HOMOs and LUMOs which are formed between carbon atoms at the surface of the C-dots and nitrogen or oxygen atoms belonging respectively to the amino groups of the polymer shell and to carboxyl groups as a rest of the citric acid used as a carbon precursor in the solution [23]. These electronic transitions are indicated in Figure 2 as n - π^*. The absorption shoulder in the visible spectral range is instead caused by a continuum of localized states at the surface of the C-dots [25]. The normalized PL spectrum of the C-dots in solution, shown in linear scale, is measured upon laser excitation at 110 mW / cm^2 and is dominated by an emission peak in the visible spectral range with maximum at 2.64 eV. The large Stokes shift of 0.76 eV can be induced by several processes, including the relaxation of the photogenerated charge carriers at surface states [25] and the formation of self-trapped excitons [26]. In Figure 3, the normalized PL spectrum of the C-dots in solution is compared to the normalized spectra of both the pristine and the functionalized devices. The pristine device was excited at 8 kW / cm^2 by focusing the laser spot onto the device on an area of 20 μm^2. For the PL measurements on the functionalized device the excitation intensity was reduced down to 150 W / cm^2 by means of a neutral density filter, in order to avoid sample degradation. The spectrum of the pristine device is characterized by two distinct emission bands. The most intense one, centered at 3.29 eV, is the near-band-edge emission (NBE) of the ZnO, which originates from excitonic recombination processes and their phonon replica [27]. The second emission band, with maximum at 2.0 eV, is the deep-level

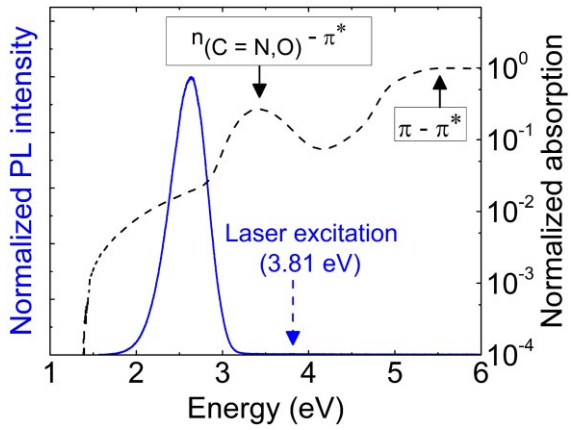

Figure 2. Absorption and photoluminescence spectra of the synthetized carbon nanodots in aqueous solution with pH 4. Both spectra are normalized with respect to the corresponding dominant peak. The absorption spectrum is shown in semi-logarithmic scale. The electronic transitions corresponding to main absorption peaks are indicated. The photoluminescence spectrum was measured under laser excitation at 3.81 eV and an intensity of 110 mW / cm^2.

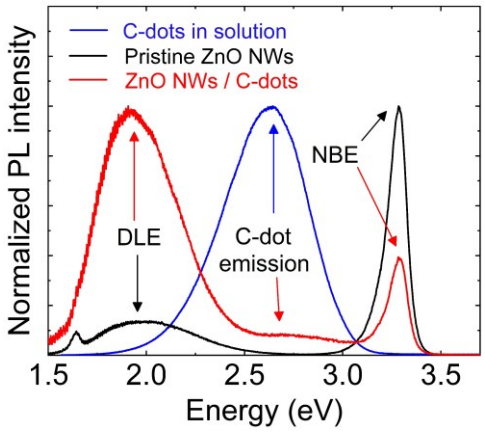

Figure 3. Photoluminescence spectra of the carbon nanodots in solution (pH 4) as well as of pristine and functionalized ZnO nanowire arrays. The spectra of the pristine and the functionalized devices were measured upon light excitation at photon energy of 3.81 eV and an excitation intensity of 12 kW / cm^2 and 40 W / cm^2, respectively.

emission (DLE) and it is caused by the radiative recombination of charge carriers at deep defect levels of the ZnO [28]. The minor peak at 1.65 eV is the second diffraction order of the NBE. The PL spectrum of the hybrid device shows both the NBE and the DLE as well as the characteristic emission band of the C-dots in solution, which appears as a shoulder of the DLE. This demonstrates the successful attachment of the C-dots to the surface of the ZnO NWs. We assume that the C-dots anchor onto the NW surface by chemical bonding between the outgoing amino groups of the C-dot stabilizer and the zinc ions at the surface of the NW [21]. Unlike the PL spectrum of the pristine device, the one of the functionalized device is dominated by the DLE. However, this cannot be conclusively attributed to an increased density of defect levels in the functionalized device. This is because the ratio between the DLE and the NBE in ZnO

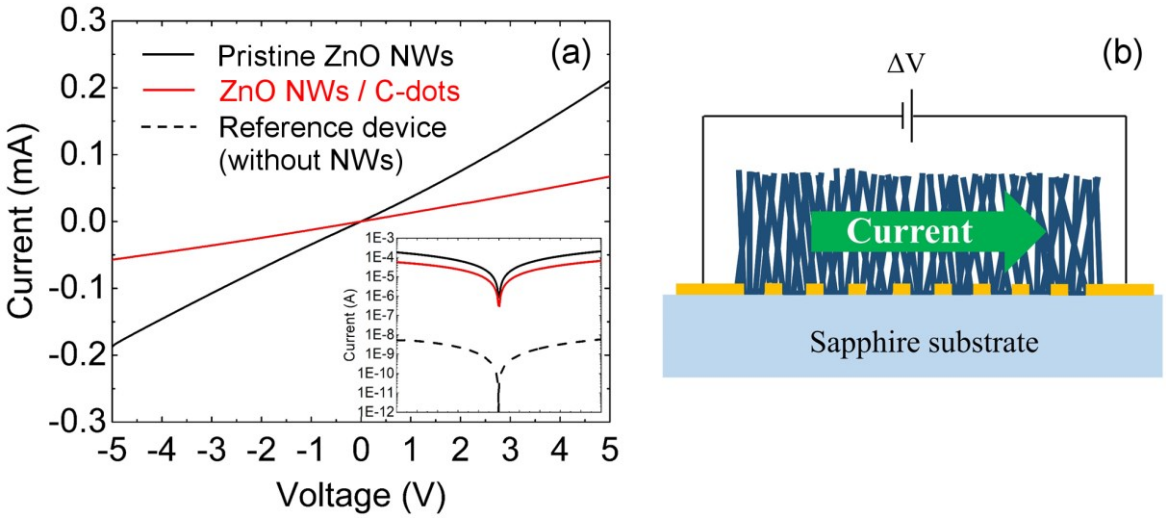

Figure 4. (a) Current - Voltage characteristics of pristine and functionalized ZnO nanowire arrays in dark. The linearity of the curves indicates the formation of Ohmic contacts. The lower conductivity of the functionalized device is attributed to the likely formation of defects at the nanowire surface occurring during functionalization. Both curves are compared in semi-logarithmic scale in the inset of the figure with the Current –Voltage characteristics of a reference device without nanowires. (b) Schematic representation of pristine device: the electric current flows through the nanowire film due to local junctions occurring between the nanowires.

depends, among other factors, also on the excitation intensity [29, 30, 31], which was adjusted at significantly different values for the PL measurements on the pristine and the functionalized devices.

The Current-Voltage (I-V) measurements on the pristine and the functionalized devices in dark are shown Figure 4 (a). The I-V characteristics are linear in both devices over a large voltage range, indicating the formation of Ohmic contacts. The lower dark conductivity of the functionalized device is attributed to the formation of defect states at the NW surface, likely occurring during the functionalization process. Additionally, both I-V characteristics are compared in the inset of the figure with those of an unfunctionalized reference device (dashed line), which was produced just with the sputtered ZnO layer but without growth of the NWs. The conductivity of the reference device is more than four orders of magnitude lower than that of the pristine

device, indicating that the ZnO seed layer itself does not play any significant role in the electron transport process because of its high resistivity. The electric current flows instead through the multiple junctions occurring between the NWs, as schematically illustrated in Figure 4 (b).

The photoconductivity properties of the hybrid devices were investigated at first under light excitation with photon energies below the band gap of ZnO in a wide spectral range from 600 nm (2.06 eV) to 390 nm (3.18 eV), in steps of 25 nm. For every measurement, the current was initially measured in dark conditions for 20 s at a voltage difference of 1 V between the device's electrodes and then for further 20 s upon light excitation at the selected excitation wavelength. An additional measurement was performed according to the same experimental procedure under light excitation at 360 nm (3.45 eV), above the band gap of ZnO. As an example, Figure 5 (a) shows the temporal dependence of the photocurrent in both the pristine and the functionalized devices under light excitation at 500 nm (2.48 eV). The photocurrent in the functionalized device rises up to 1.06 μA within 20 s, whereas it reaches only 0.14 μA within the same temporal interval in the pristine one. Both curves can be well described by an empirical function $I_{ph} \propto t^{\alpha}$. The obtained values of α (0.3 and 0.8 for the pristine and the functionalized device, respectively) indicate that the temporal dependence of the photocurrent in the pristine device has a more pronounced sublinear character than in the functionalized one. The photocurrent generated in both devices was then calculated as the difference between the maximum current under light excitation and the dark current, and is plotted as a function of the selected photon energy in Figure 5 (b). The pristine sample shows poor photoresponse in the visible spectral range, which is attributed to the excitation of defect levels in the ZnO. A drastic increase of the photocurrent is observed above 3.1 eV due to the direct photoexcitation of electrons from the valence to the conduction band of ZnO. As a remark, the direct photogeneration of charge carriers at this photon energy threshold below the band gap of the ZnO (3.37 eV) is allowed by the non-negligible spectral width of the light beam selected by the monochromator.

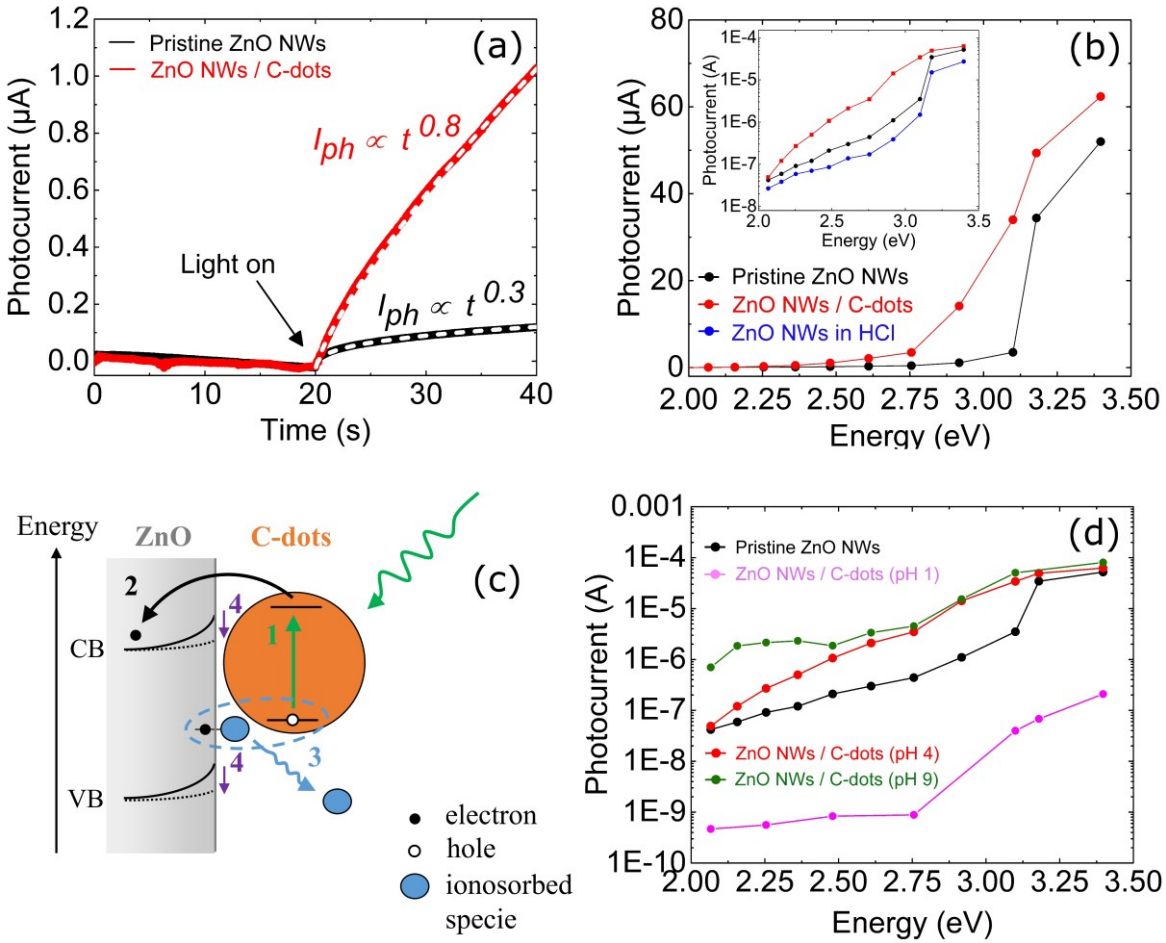

Figure 5. (a) Temporal dependence of the photocurrent in pristine and functionalized ZnO nanowire arrays under light excitation at 500 nm (2.48 eV). Fitting functions $I_{ph} \propto t^{\alpha}$ are indicated by white dashed lines. (b) Photocurrent in both devices as a function of the exciting photon energy. Both curves are compared in semi-logarithmic scale in the inset of the figure with that from a reference device without carbon nanodots, which was treated in an aqueous solution of HCl with the same pH 4 of the functionalizing solution. (c) Model for the photoconductivity enhancement in the functionalized device upon light excitation with photon energies below the band gap of ZnO. The main steps of the process are indicated: (1) absorption of the incident photons in the C-dots and excitation of the electrons from the HOMO to the LUMO; (2) injection of the photoexcited electrons into the conduction band of the ZnO nanowire; (3) Desorption of ionosorbed species from the ZnO surface favored by their electrostatic interaction with the holes left in the C-dots; (4) Consequent reduction of the surface band bending. (d) Photocurrent as a function of the exciting photon energy in ZnO nanowire arrays functionalized with carbon nanodots in aqueous solutions with different pH values.

On the other hand, the functionalized device shows enhanced photoresponse within the inves-

tigated spectral range, as particularly evident on a logarithmic scale in the inset of Figure 5 (b). Additionally, in the inset the photocurrent of both devices is compared with that of a reference device, which was treated in an aqueous solution of HCl not containing the C-dots but with the same pH value 4 of the functionalizing solution. Since the reference device shows a lower photoconductivity than the pristine one, we can exclude a direct influence of the aqueous solution on the enhanced photoresponse of the functionalized devices, which can be instead mainly attributed to the attachment of the C-dots on the surface of the ZnO NWs.

As schematically illustrated in Figure 5 (c), we suggest that the photocurrent enhancement observed in the functionalized device originates from the co-occurrence of a fast injection of photoexcited electrons from the C-dots into the conduction band of the ZnO NWs (with temporal scales ranging from ps to ns [16, 17]), and other surface processes characterized by a slower temporal dynamics. The injection process occurs after the photoexcitation of electrons from HOMOs to LUMOs in correspondence to the carboxyl and amino groups at the surface of the C-dots, which are mainly involved in the electronic transitions in the investigated spectral range below the band gap of ZnO (Figure 2). Because of this electron injection, unbalanced holes are left in the HOMO of the surface C-dots, which can electrostatically interact with negatively charged adsorbed species such as O_2^- and OH^-, typically present at the surface of ZnO NWs in the proximity of surface defects [32]. It is well known that such adsorbed species trap electrons from the conduction band of ZnO, inducing the pinning of the Fermi level at the surface and the corresponding formation of a surface band bending in the NWs [32, 33]. The electrostatic interaction between the holes left in the C-dots after the electron injection and these negatively charged ionic species may weaken their adsorption bonds, eventually favoring their desorption and a partial discharge of the NW surface. Therefore, the fast injection of photoexcited electrons from the C-dots into the conduction band of the ZnO NWs does not only induce a quick increase of the device photoconductivity thanks to the enhanced electron density in the NWs, but causes indirectly also a reduction of the NW surface band bending, which leads to a further increase

of the device photoconductivity. The latter contribution proceeds on a significantly longer temporal scale than the electron injection into the NWs, since it is driven by the slow desorption dynamics of the chemical species from the surface of ZnO [34, 8, 16], and accounts for the slow temporal dynamics of the photocurrent increase observed in the functionalized device (Figure 5 (a)).

Since the electrical properties of ZnO NWs are also affected by the pH value of the surrounding environment [35, 36, 37], we measured the wavelength-resolved photocurrent in three different devices, functionalized according to the previously described procedure in aqueous solutions with the same concentration of C-dots (0.08 % in mass) but different pH values. Compared to the pristine device, the photoresponse enhancement observed in the device functionalized in the solution with pH 9 is slightly higher than that observed in the device with pH 4, in particular at low exciting photon energy (Figure 5 (d)). On the other hand, the device with pH 1 has a drastically lower photoconductivity than the pristine one. This indicates that increasing the acidity of the prepared solution is deleterious for the photoresponse performance of the investigated ZnO NW devices.

Furthermore, we performed photoconductivity measurements under light excitation with photon energy above the band gap of ZnO, in order to investigate the temporal dynamics of the device photoresponse and the photoconductivity decay. The measurements were performed with a He-Cd laser as a light excitation source at different excitation intensities, ranging from 0.2 mW / cm^2 up to 51 mW / cm^2. The current was measured at a voltage difference of 1 V between the device´s electrodes. For every measurement, the current was initially measured in dark conditions and then for two hours upon light excitation. After removing the illumination the current was recorded for further 16 hours. The measurements performed on the pristine and the functionalized devices are shown respectively in Figure 6 (a) and 6 (b). In the pristine device

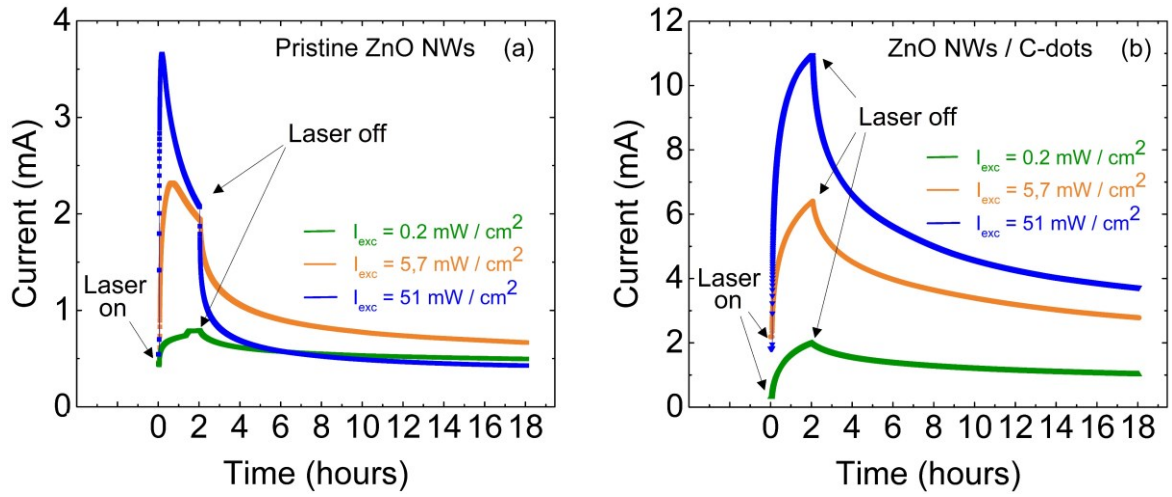

Figure 6. Temporal dependence of the photocurrent in pristine (a) and functionalized ZnO nanowire arrays (b) under laser excitation at photon energy of 3.81 eV and various excitation intensities.

the current increases quickly as soon as the laser excitation is switched on. At the lowest excitation intensity, the current increase tends to saturate within two hours, while upon excitation at higher light intensities the current reaches initially a maximum and then progressively drops. After removing the excitation, the decay of the current speeds up. The drop of the current observed during excitation at 5.7 mW / cm^2 and 51 mW / cm^2 amounts to 20 % and 50 %, respectively, of the corresponding maximum value of the current. On the other hand, this effect has not been observed in the functionalized device, in which the current increases continuously upon excitation at all investigated values of the light intensity. The drop of the current observed during light excitation in the pristine device has been already reported to occur in contacted single ZnO NWs and thin films and can be attributed to the decrease of the charge carrier density as a result of an electron trapping process at the surface [38, 39]. It is widely accepted that upon light excitation with photon energy above the band gap, photogenerated electrons and holes in ZnO NWs are physically separated due to the upward surface band bending, which originates from the previously mentioned pinning of the Fermi level at the NW surface [40, 33].

Specifically, the photogenerated holes tend to migrate towards the surface, while unpaired electrons remain in the core of the NW with prolonged lifetime, giving origin to a pronounced increase of the photoconductivity. At the surface, the accumulated holes recombine with electrons previously trapped at surface states, inducing a partial discharge of the surface and a corresponding reduction of the surface band banding. If the reduction of the surface band bending becomes significant, a non-negligible fraction of the photogenerated electrons can overcome the energy barrier associated with the band bending even during light excitation, getting trapped at the surface and inducing a drop of the NW photoconductivity. Since the amplitude of the discharge of the surface and the corresponding reduction of the surface band banding are likely proportional to the density of photogenerated holes, the drop of the photocurrent during light excitation is expected to be proportional to the excitation intensity. This explains the experimental evidence, that the drop of the photoconductivity observed during the illumination in the pristine device becomes larger for increasing excitation intensity. Additionally, since the electron trapping at the ZnO surface is particularly favored by the simultaneous adsorption of oxygen molecules from the surrounding environment [32, 41, 42], the absence of a photoconductivity drop during light excitation in the hybrid device indicates the limited access of oxygen molecules to the NW surface as a consequence of their surface passivation.

The above-band-gap photoresponse of both devices is quantitatively described in terms of the photoresponsivity, which was calculated as the ratio between the maximum generated photocurrent and the excitation intensity. As shown in Figure 7, the functionalized device has higher photoresponsivity than the pristine one within the investigated range of excitation intensities. This is attributed to the fact that at the exciting photon energy of 3.81 eV both the ZnO NWs and the C-dots can absorb the light and contribute to the device photoconductivity. The decrease of the photoresponsivity for increasing excitation intensity, observed in both devices, indicates the progressive saturation of the photocurrent enhancement. In the pristine device, this results from the impact of the light-induced modulation of the surface band bending in ZnO NWs on

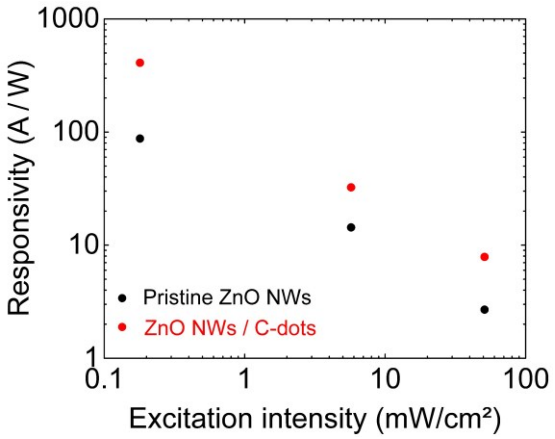

Figure 7. Photoresponsivity of pristine and functionalized ZnO nanowire arrays upon laser excitation at photon energy of 3.81 eV, as a function of the excitation intensity.

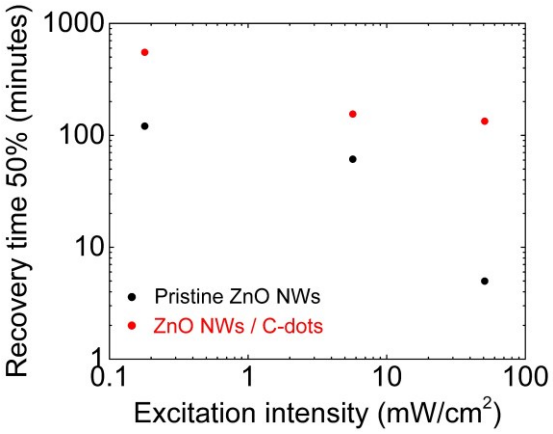

Figure 8. Recovery times required to achieve 50 % of the photocurrent decay in pristine and functionalized ZnO nanowire arrays after laser excitation at photon energy of 3.81 eV, as a function of the excitation intensity.

the lifetime of the photogenerated charge carriers. Specifically, as the excitation intensity increases, the discharge of the NW surface and the corresponding reduction of the surface band bending upon light excitation become progressively more pronounced, leading to a less efficient spatial separation of the electron - hole pairs and an increasing recombination probability of the photogenerated charge carriers. As a result, this process limits further enhancements of the photocurrent. Also in the C-dots the electron-hole recombination probability is expected to increase with the excitation intensity, due to the high spatial confinement experienced by the photoexcited electrons in the LUMOs of such low dimensional material system. This leads to a progressive reduction of the efficiency of the electron injection into the conduction band of the ZnO NWs, which induces the observed decrease of the photoresponsivity in the functionalized device.

The decay of the photocurrent after light excitation proceeds in both samples on the temporal scale of several hours (Figures 6 (a) and 6 (b)). Within 16 hours after removing the laser exci-

tation, the original dark current is completely recovered only in the pristine device after excitation at intensity of 0.2 mW / cm^2. For this reason, we limited the investigation of the temporal dynamics of the charge carrier relaxation to the time required to observe 50 % of the photocurrent decay. Figure 8 shows the corresponding recovery times observed in both devices as a function of the excitation intensity. After laser excitation at intensities ranging from 0.2 mW / cm^2 up to 51 mW / cm^2, the recovery times in the pristine device range respectively from 120 minutes up to 5 minutes. Significantly longer decays have been observed in the functionalized device within the same range of excitation intensities. The slow decay of the photocurrent in ZnO nanostructures is known as persistence of the photoconductivity and is typically attributed to the slow relaxation of photogenerated electrons by surface trapping, assisted by adsorption of oxygen molecules from the surrounding environment [32, 41, 42]. The enhanced persistence of the photoconductivity in the functionalized device can therefore be ascribed to the limited access of oxygen molecules to the surface of the functionalized NWs, which leads to a reduced rate of the photoelectron relaxation by surface trapping.

Taken together, our results demonstrate the possibility to successfully functionalize ZnO NWs with environmentally benign and low-cost C-dots, in order to enhance their photoresponse properties in the visible spectral range. In particular, combined optical and photoconductivity measurements clearly reveal that, in this spectral range, the electron photoexcitation mainly occur at the surface of the C-dots, which is passivated by the polymer ligand molecules. This opens up novel perspectives regarding the engineering of the surface of the C-dots, which may lead to the achievement of further device functionalities as well as remarkable contributions towards the development of a sustainable “green optoelectronics”.

Conclusions

In summary, we have investigated the photoconductivity properties of hybrid nanostructured devices consisting of a ZnO NW array, functionalized with C-dots. We have shown that the surface functionalization of the NW leads to an increase of the device photoresponse in the visible spectral range, as well as enhanced UV photoconductivity. This is attributed to the fast injection of photoexcited electrons from the C-dots into the conduction band of the NWs, and the subsequent slower desorption of molecular species from the NW surface, which reduces the surface depletion region in the NWs. Furthermore, we have investigated the temporal dynamics of the photoconductivity decay after UV excitation. In comparison to the pristine devices, significantly longer decay has been observed in the functionalized ones, which is attributed to a reduced rate of the photoelectron relaxation by surface trapping because of the surface passivation in the functionalized ZnO NWs.

Acknowledgments

We gratefully acknowledge Angelika Schmidt for the support in the synthesis of the ZnO nanowires. Furthermore, we gratefully acknowledge support of the Braunschweig International Graduate School of Metrology B-IGSM and the DFG Research Training Group GrK1952/1 "Metrology for complex Nanosystems", the DFG research unit FOR1616 as well as the European Union's Seventh Framework Program (FP/2007-2013)/ERC Grant Agreement n. 336917. J.D. Prades acknowledges the support from the Serra Húnter Program.

References

[1] R. Yan, D. Gargas and P. Yang, "Nanowire photonics," *Nat. Photonics,* vol. 3, no. 10, pp. 569-576, 2009.

[2] S. Rühle, M. Shalom and A. Zaban, "Quantum-Dot-Sensitized- Solar Cells," *ChemPhysChem,* vol. 11, no. 11, pp. 2290-2304, 2010.

[3] A. Kolmakov, D. O. Klenov and Y. Lilach, "Enhanced gas sensing by individual sno2 nanowires and nanobelts functionalized with pd catalyst particles," *Nano Lett,* vol. 5, no. 4, pp. 667-673, 2005.

[4] R. Niepelt, U. C. Schröder, J. Sommerfeld, I. Slowik, B. Rudolph, R. Möller, B. Seise, A. Csaki, W. Fritzsche and C. Ronning, "Biofunctionalization of zinc oxide nanowires for dna sensory applications," *Nanoscale Res. Lett,* vol. 6, no. 511, pp. 1-7, 2011.

[5] A. Pescaglini and D. Iacopino, "Metal nanoparticle–semiconductor nanowire hybrid nanostructures for plasmon-enhanced optoelectronics and sensing," vol. 3, no. 45, pp. 11785-11800, 2015.

[6] B. O'Regan and M. A. Grätzel, "A Low-Cost, High-Efficiency Solar Cell Based on Dye Sensitized Colloidal TiO2 Films," *Nature,* vol. 353, no. 6346, p. 737−740, 1991.

[7] X. Zhang, F. Wang, H. Huang, H. T. Li, X. Han, L. Y. and Z. H. Kang, "Carbon quantum dot sensitized TiO2 nanotube arrays for photoelectrochemical hydrogen generation under visible light," *Nanoscale,* vol. 5, no. 6, pp. 2274-2278, 2013.

[8] D. Hou, A. Dev, K. Frank, A. Rosenauer and T. Voss, "Oxygen-Controlled Photoconductivity in ZnO Nanowires Functionalized with Colloidal CdSe Quantum Dots," *J. Phys. Chem. C ,* vol. 116, no. 36, pp. 19604-19610, 2012.

[9] A. Pescaglini, A. Martin, D. Cammi, G. Juska, C. Ronning, E. Pelucchi and D. Iacopino, "Hot-Electron Injection in Au Nanorod/ZnO Nanowire Hybrid Device for Near-Infrared Photodetection," *Nano Lett ,* vol. 14 , no. 11, pp. 6202-6209, 2014.

[10] A. Janotti and C. G. Van de Walle, "Fundamentals of zinc oxide as a semiconductor," *Rep. Prog. Phys,* vol. 72, no. 12, pp. 126501-29, 2009.

[11] Ü. Özgür, D. Hofstetter and H. Morkoç, "Zno devices and applications: a review of current status and future prospects," *Proc. IEEE ,* vol. 98, no. 7, pp. 1255-1268, 2010.

[12] E. Comini, C. Baratto, G. Faglia, M. Ferroni, A. Ponzoni, D. Zappa and G. Sberveglieri, "Comini, E.; Baratto, C.; Faglia, G.; Ferroni, M.; Ponzoni, A.; Zappa, D.; Sberveglieri, G. Metal oxide nanowire chemical and biochemical sensors," *J. Mater. Res,* vol. 28, no. 21, pp. 2911-2931, 2013.

[13] A. P. Alivisatos, "Semiconductor Clusters, Nanocrystals, and Quantum Dots.," *Science,* vol. 271 , no. 5251, pp. 933-937, 1996.

[14] R. Koole, E. Groeneveld, D. Vanmaekelbergh, A. Meijerink and C. d. M. D. C. de Mello Donegá, "(ed.), Nanoparticles – Workhorses of Nanoscience. 2014, pp. 13 – 51 (Part of book).".

[15] C. Smith and D. Binks, "Smith, C.; Binks, D.; Multiple Exciton Generation in Colloidal Nanocrystals," *Nanomaterials,* vol. 4, no. 1, pp. 19-45, 2014.

[16] S. Bley, M. Diez, F. Albrecht, S. Resch, S. Waldvogel, A. Menzel, M. Zacharias, J. Gutowski and T. Voss, "Electron Tunneling from Colloidal CdSe Quantum Dots to ZnO Nanowires Studied by Time-Resolved Luminescence and Photoconductivity Experiments.," *J. Phys. Chem. C,* vol. 119, no. 27, pp. 15627-15635, 2015.

[17] K. Zídek, K. Zheng, C. Ponseca Jr., M. Messing, L. R. Wallenberg, P. Chabera, M. Abdellah, V. Sundström and T. Pullerits, "Chabera, P.; Abdellah, M.; Sundström, V.; Pullerits, T. Electron Transfer in Quantum-Dot-Sensitized ZnO Nanowires: Ultrafast Time-Resolved Absorption and Terahertz Study," *J. Am. Chem. Soc,* vol. 134, no. 29, pp. 12110-12117, 2012.

[18] S. Y. Lim, W. Shen and Z. Gao, "Carbon quantum dots and their applications," *Chem. Soc. Rev. ,* vol. 44, no. 1, pp. 362-381, 2015.

[19] X. Li, M. Rui, J. Song, Z. Shen and H. Zeng, " Li, X.; Rui, M.; Song, J.; Shen, Z.; Zeng, H. Carbon and Graphene Quantum Dots for Optoelectronic and Energy Devices: A Review," *Adv. Funct. Mater,* vol. 25, no. 31, pp. 4929-4947, 2015.

[20] H. Li, Z. Kang, Y. Liu and S.-T. Lee, "Carbon nanodots: synthesis, properties and applications," *J. Mater. Chem,* vol. 22, no. 46, p. 24230–24253, 2012.

[21] A. Dominguez, M. Lorke, A. L. Schoenhalz, A. L. Rosa, T. Frauenheim, A. R. Rocha and G. M. Dalpian, "First principles investigations on the electronic structure of anchor groups on ZnO nanowires and surfaces," *J. Appl. Phys,* vol. 115, no. 20, pp. 203720-9, 2014 .

[22] M. W. G. Hoffmann, A. E. Gad, J. D. Prades, F. Hernández-Ramírez, R. Fiz, H. Shen and S. Mathur, "Solar Diode Sensor: Sensing Mechanism and Applications," *Nano Energy,* vol. 2, no. 4, pp. 514-522, 2013.

[23] S. Hu, A. Trinchi, P. Atkin and I. Cole, "Tunable Photoluminescence Across the Entire Visible Spectrum from Carbon Dots Excited by White Light," *Angew. Chem. Int. Ed,* vol. 54, no. 10, pp. 2970-2974, 2015.

[24] N. H., M. Li, L. Q., S. Liang, Y. Tan, L. Sheng, W. Shi and S. X.-A. Zhang, "Carbon Dots with Continuously Tunable Full-Color Emission and Their Application in Ratiometric pH Sensing," *Chem. Mater,* vol. 26, no. 10, pp. 3104-3112, 2014.

[25] S. Zhu, Y. Song, X. Zhao, J. Shao, J. Zhang and B. Yang, "The photoluminescence mechanism in carbon dots (graphene quantum dots, carbon nanodots, and polymer dots): Current state and future perspective," *Nano Res,* vol. 8, no. 2, pp. 355-381, 2015.

[26] M. Fu, F. Ehrat, Y. Wang, K. Z. Milowska, C. Reckmeier, A. L. Rogach, J. K. Stolarczyk, A. S. Urban and F. J., "Carbon Dots: A Unique Fluorescent Cocktail of Polycyclic Aromatic Hydrocarbons," *Nano Lett,* vol. 15, no. 9, pp. 6030-6035, 2015.

[27] B. K. Meyer, H. Alves, D. M. Hofmann, W. Kriegseis, D. Forster, F. Bertram, J. Christen, A. Hoffmann, M. Straßburg, M. Dworzak, U. Haboeck and A. V. Rodina, "Bound exciton and donor-acceptor pair recombinations in zno," *Phys. Status Solidi B,* vol. 241, no. 2, pp. 231-260, 2004.

[28] S. Müller, M. Lorenz, C. Czekalla, G. Benndorf, H. Hochmuth, M. Grundmann, H. Schmidt and C. Ronning, "Intense white photoluminescence emission of V-implanted zinc oxide thin films," *J. Appl. Phys,* vol. 104, no. 12, pp. 123504-7, 2008.

[29] X. H. Zhang, S. J. Chua, A. M. Yong, H. Y. Yang, S. P. Lau, S. F. Yu, X. W. Sun, L. Miao, M. Tanemura and S. Tanemura, "Exciton radiative lifetime in ZnO nanorods fabricated by vapor phase transport method," *Appl. Phys. Lett,* vol. 90, no. 1, p. 013107–3, 2007.

[30] M. A. Reshchikov, "Defects in bulk ZnO studied by steady-state and time-resolved photoluminescence," *Mater Res Soc Symp Proc.*

[31] D. Hou, T. Voss, C. Ronning, A. Menzel and M. Zacharias, "Deep-level emission in ZnO nanowires and bulk crystals: Excitation-intensity dependence versus crystalline quality," *J. Appl. Phys. ,* vol. 115, no. 23, pp. 233516-7, 2014.

[32] D. A. Melnick, "Zinc oxide photoconduction, an oxygen adsorption process," *J. Chem. Phys,* vol. 26, no. 5, pp. 1136-1146, 1957.

[33] C. Y. Chen, J. R. D. Retamal, I. W. Wu, D. H. Lien, M. W. Chen, Y. Ding, Y. L. Chueh, C. I. Wu and J. H. He, "Probing surface band bending of surface-engineered metal oxide nanowires," *ACS Nano ,* vol. 6, no. 11, pp. 9366-9372, 2012.

[34] S. V. Andersen, V. Vandalon, R. H. E. C. Bosch, B. W. H. van de Loo, K. Pedersen and W. M. M. Kessels, "Interaction between O2 and ZnO films probed by time-dependent second-harmonic generation," *Appl. Phys. Lett.,* vol. 104, no. 5, pp. 051602-5, 2014.

[35] A. Menzel, K. Subannajui, F. Güder, D. Moser, O. Paul and M. Zacharias, "Multifunctional ZnO-Nanowire-Based Sensor," *Adv. Funct. Mater. ,* vol. 21, no. 22, pp. 4342-4348, 2011.

[36] V. Cauda, P. Motto, D. Perrone, G. Piccinini and D. Demarchi, "pH-triggered conduction of amine-functionalized single ZnO wire integrated on a customized nanogap electronic platform," *Nanoscale Res. Lett. ,* vol. 9, no. 1, pp. 53-10, 2014.

[37] B. S. Kang, F. Ren, Y. W. Heo, L. C. Tien, D. P. Norton and S. J. Pearton, "pH measurements with single ZnO nanorods integrated with a microchannel," *Appl. Phys. Lett.,* vol. 86, no. 11, pp. 112105-3, 2005.

[38] S.-W. Fan, A. K. Srivastava and V. P. Dravid, "UV-activated room-temperature gas sensing mechanism of polycrystalline ZnO," *Appl. Phys. Lett,* vol. 95, no. 14, pp. 142106-3, 2009.

[39] M.-W. Chen, J. R. D. Retamal, C. Y. Chen and J. H. He, "Photocarrier Relaxation Behavior of a Single ZnO Nanowire UV Photodetector: Effect of Surface Band Bending," *IEEE Electron Device Lett,* vol. 33, no. 3, pp. 411-413, 2012.

[40] A. Soudi, C.-H. Hsu and Y. Gu, "Diameter-dependent surface photovoltage and surface state density in single semiconductor nanowires," *Nano Lett,* vol. 12, no. 10, pp. 5111-5116, 2012.

[41] D. Cammi and C. Ronning, "Persistent photoconductivity in zno nanowires in different atmospheres," *Adv. Cond. Matter Phys,* vol. 2014 (Article ID 184120), 2014.

[42] J. Bao, I. Shalish, Z. Su, R. Gurwitz, F. Capasso, X. Wang and Z. Ren, "Photoinduced oxygen release and persistent photoconductivity in zno nanowires," *Nanoscale Res. Lett,* vol. 6, no. 404, pp. 1-7, 2011.